Semiconductive 3D Phthalocyanine Metal-Catecholates for High Electrochemical Carbon Dioxide Reduction

Roc Matheu,[†] Enrique Gutierrez-Puebla,[‡] M. Ángeles Monge,[‡] Christian S. Diercks,[†] Joohoon Kang,[†,§] Mathieu S. Prévot,[†] Xiaokun Pei,[†] Nikita Hanikel,[†] Bing Zhang,[†] Peidong Yang,[†] Omar M. Yaghi*[,†,⊥]

[†] Department of Chemistry, University of California-Berkeley; Materials Sciences Division, Lawrence Berkeley National Laboratory; and Kavli Energy NanoSciences Institute, Berkeley, California 94720, United States

[‡] Department of New Architectures in Materials Chemistry, Instituto de Ciencia de Materiales de Madrid, Consejo Superior de Investigaciones Científicas, Madrid 28049, Spain

[⊥] UC Berkeley-KACST Joint Center of Excellence for Nanomaterials for Clean Energy Applications, King Abdulaziz City for Science and Technology, Riyadh 11442, Saudi Arabia

Supporting Information Placeholder

ABSTRACT: The synthesis of a new anionic 3D metal-catecholate framework, termed MOF-1992, is achieved by linking tetratopic cobalt phthalocyanin-2,3,9,10,16,17,23,24-octaol linkers with $Fe_3(-C_2O_2-)_6(OH_2)_2$ trimers into an extended framework of **roc** topology. MOF-1992 exhibits sterically accessible Co active sites together with semiconductive properties (5.7×10^{-5} S cm^{-1}). Cathodes based on MOF-1992 and carbon black (CB) display a high coverage of electroactive sites (270 nmol cm^{-2}) and a high current density (−16.5 mA cm^{-2}; overpotential, -0.52 V) for the CO_2 to CO reduction reaction in water (faradaic efficiency, 80%). Over the six-hour experiment, MOF-1992/CB cathodes reach turnover numbers of 5,800 with turnover frequencies of 0.20 s^{-1} per active site.

The electrochemical reduction of CO_2 to energy-rich carbon compounds promises a route to carbon-neutral energy.[1] Metal complexes and inorganic solids have been found to catalyze the reduction of CO_2.[2] Cathodes based on inorganic solids catalytically reduce CO_2 at high current densities due to their intrinsic fast electron transport properties and concomitant high number of catalytically active sites.[3] In contrast, tuning of homogeneous molecular catalysts has allowed for increased selectivity[4] and specific activity[5] in the CO_2 reduction reaction to an extent unprecedented for inorganic solids.[6,7] The outstanding challenge for cathodes based on discrete metal complexes is, however, to achieve high electroactive catalyst loading in order to generate high current densities.[8,9,10,11] Metal–organic frameworks (MOFs) and covalent organic frameworks (COFs) — reticular frameworks— are an attractive class of solids in this regard because molecular CO_2 reduction catalysts can be used as building blocks to generate porous extended structures.[12] Cathodes based on reticular frameworks have achieved high selectivity and improved activity for catalytic CO_2 reduction.[13] However, the low conductivity or inaccessible sites of the large majority of existing frameworks have, thus far, prevented to reach current densities comparable to those of inorganic solids.[14,15,16,17,18] Hence, the main challenge for reticular chemistry with regard to CO_2 reduction is to create conductive frameworks that contain accessible molecular catalysts as part of the backbone.

To address this goal we turned our attention to 3D metal-catecholate frameworks, a class of MOFs that are constructed through metal-catecholate linkages.[19] In contrast to the archetypical carboxylate-based MOFs, metal-catecholates display electron transport due to favorable orbital overlap between the metal ion (e.g. Fe, V) and the catechol.[20,21,22] Here, a new 3D anionic metal-catecholate framework $[Fe_6(OH_2)_4(CoPc)_3]^{6-}$, termed MOF-1992, is constructed from Co-phthalocyanine catechol linkers (cobalt phthalocyanin-2,3,9,10,16,17,23,24-octaol, CoPc), a known molecular CO_2-reduction catalyst,[8,9,11,23,24] and $Fe_3(-C_2O_2-)_6(OH_2)_2$ trimers (Figure 1). The combination of semiconductive properties and accessible active sites in MOF-1992 results in cathodes that reduce CO_2 at a current density of −16.5 mA cm^{-2} at -0.52 V of overpotential in water, a performance one order of magnitude higher than that of cathodes based on previously reported reticular frameworks.

MOF-1992•$[Fe]_3$ was prepared by dissolving $FeCl_2$ and CoPc in a solvent mixture of *N,N*-dimethylformamide/water/methanol (100/0.5/0.5, v/v) in a borosilicate tube, which was placed in an oven at 150 °C for 16 h. Black rod-shaped crystals

with homogeneous morphology and of suitable size for single crystal X-ray diffraction analysis were isolated (Figure 2a). The single crystal structure of MOF-1992 was solved in the tetragonal space group $I4_1/amd$ (No. 141) with the lattice parameters a = 29.121 Å and c = 52.191 Å. Each CoPc is coordinated to four $Fe_3(\text{-}C_2O_2\text{-})_6(OH_2)_2$ trimers through the catecholate oxygens to generate an open 3D framework of previously unreported **roc** topology (Figure 1 and S4). MOF-1992 features a square-shaped channel of 14.5 Å in diameter along the c axis (Figure 1 and S3, accessible space). In contrast to other reticular frameworks based on phthalocyanine linkers, the CoPc units of MOF-1992 do not interact by π- π stacking but instead face the interior of this 1D channel.[25,26,27,28] This improves the accessibility of the catalytic CoPc sites. Two additional channels along a, 10 Å and 5 Å in diameter, respectively (Figure 1 and S3), contribute to the highly interconnected 3D pore structure.

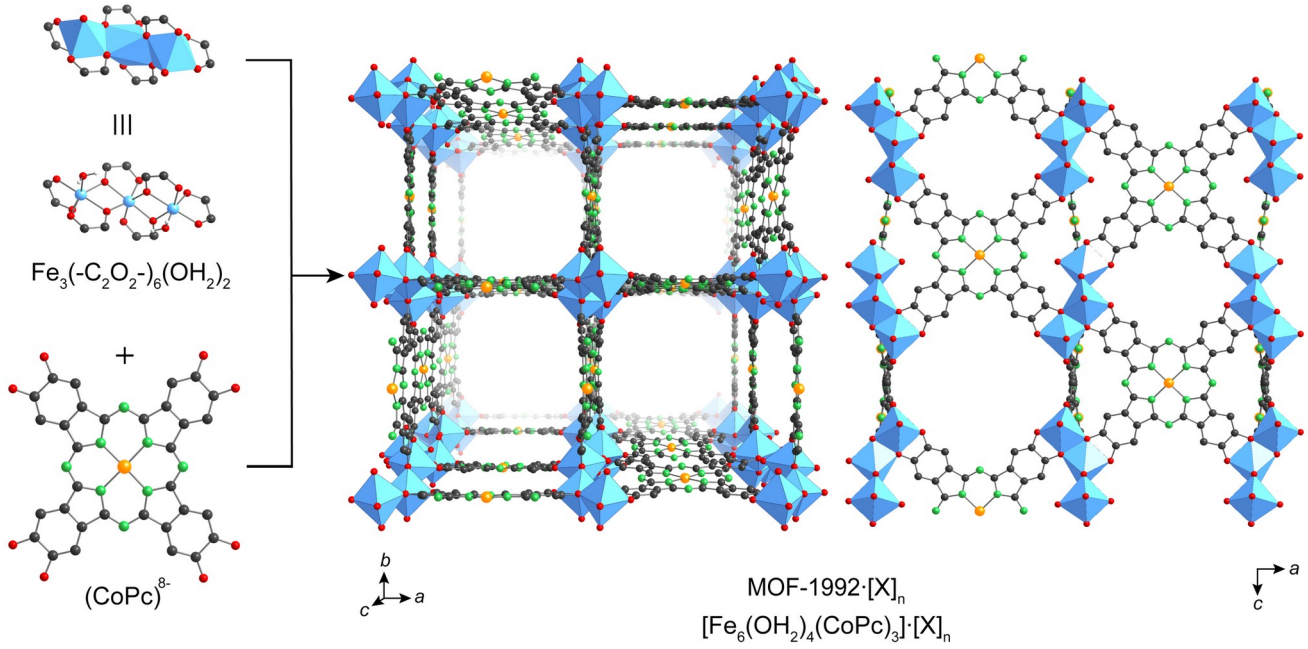

Figure 1. Single crystal X-ray structure of MOF-1992 based on Fe trimers and Co phthalocyanine catechol linkers (CoPc). Atom color scheme: C, black; O, red; N, green; Co, orange; Fe, blue polyhedra. Hydrogen atoms and chlorido ligands (Section S3) are omitted. The anionic charge of $[Fe_6(OH_2)_4(CoPc)_3]^{6-}$, MOF-1992, is balanced by the presence of $[X]_n$ counterions (X = Mg^{2+} or Fe^{3+}).

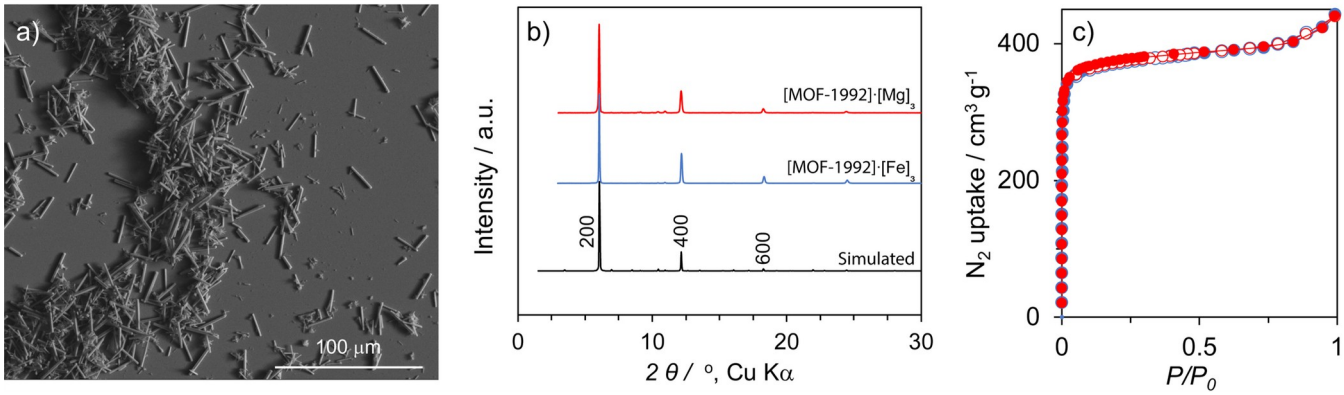

Figure 2. a) SEM image of MOF-1992•$[Fe]_3$. b) Simulated (black) and experimental PXRD patterns for MOF-1992•$[Fe]_3$ (blue) and MOF-1992•$[Mg]_3$ (red). c) N_2 sorption isotherm at 77 K for MOF-1992•$[Fe]_3$ and MOF-1992•$[Mg]_3$; P, system pressure; P_0, saturation pressure.

The chemical formula for MOF-1992•$[Fe]_3$ was elucidated by a combination of Mössbauer spectroscopy, inductively coupled plasma atomic emission spectroscopy (ICP-AES), x-ray photoelectron spectroscopy (XPS) and elemental microanalysis. Activated MOF-1992•$[Fe]_3$ was prepared by solvent exchange with *N*,*N*-dimethylformamide (DMF) and anhydrous methanol, followed by evacuation under dynamic vacuum. Mössbauer spectroscopy showed that only high spin Fe^{3+} was present in the structure while Co^{2+} was found by XPS (Sections S8-S9). ICP-AES was used to decipher the ratio of Fe:Co in the structure which was found to be 3:1 (Table S2). As such, these

measurements yield a chemical formula of $[Fe_6(OH_2)_4(CoPc)_3]\bullet[Fe_3(OH)_3(OH_2)_2]$, MOF-1992•$[Fe]_3$. In the chemical formula, six Fe^{3+} form part of two $Fe_3(\text{-}C_2O_2\text{-})_6(OH_2)_2$ trimers and three Fe^{3+} act as counter ions that compensate for the negative charge of the framework. To further corroborate the existence of the counterions inside the structure, the Fe^{3+} countercations in MOF-1992•$[Fe]_3$ were post-synthetically replaced by Mg^{2+} by dispersing the MOF in a $MgCl_2$ solution in DMF at 100 °C. The resulting crystals were thoroughly washed with DMF and methanol before evacuation to yield $[Fe_6(OH_2)_4(CoPc)_3]\bullet[Mg_3(OH_2)_3]$, MOF-1992•$[Mg]_3$ (Section S2). Powder X-ray diffraction (PXRD) of MOF-1992•$[Fe]_3$ and MOF-1992•$[Mg]_3$ showed identical diffraction patterns (Figure 2b) and scanning electron microscopy (SEM) showed analogous crystal morphology (Figure S5). In addition, ICP-AES confirmed the quantitative cation exchange (Table S2).

N_2 gas sorption isotherms at 77 K assessed the permanent porosity of the frameworks (Figure 2c). The Brunauer−Emmett−Teller (BET) areas for MOF-1992•$[Fe]_3$ and MOF-1992•$[Mg]_3$ were calculated to be 1471 and 1481 $m^2\ g^{-1}$ respectively, corresponding to ~ 75 % of the theoretical surface areas; based on the single crystal structure without cations (Section S11). The pore size distribution also remained largely unaffected by the counterion exchange (Table S3).

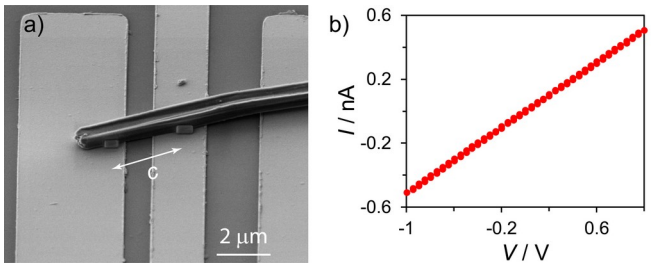

Figure 3. a) SEM image showing a crystal of MOF-1992•$[Mg]_3$ on a pre-patterned Au electrode. b) Conductivity measurement for MOF-1992•$[Mg]_3$ at 298 K.

MOF-1992•$[Mg]_3$ was chosen to determine the conductivity of the MOF-1992 backbone, as Mg^{2+} is a redox innocent counterion. We transferred crystals of MOF-1992•$[Mg]_3$ onto pre-patterned Au bottom electrodes using a micromanipulator and, for improved contact between the electrode and MOF-1992•$[Mg]_3$, Pt was deposited at the MOF/electrode interface by electron beam induced deposition (Figure 3a).[29] The *I/V* curve for MOF-1992•$[Mg]_3$ (Figure 3b) shows linear behavior and a conductivity of 5.7×10^{-5} S cm^{-1}.[21] The conductivity value may be underestimated due to unknown resistance in the contact and the two-point probe method used in this conductivity measurement (Section S7).[22] The conductivity measurement was performed along the rod, and thus along the *c* axis of the structure (Figure 1), according to the observed preferential orientation by PXRD (Figure S7). The measurements thus indicate that the electron transfer pathway passes through both the $Fe_3(\text{-}C_2O_2\text{-})_6(OH_2)_2$ trimers and the phthalocyanine linkers (Figure 1). In addition, the cyclically localized pi electrons of the phthalocyanine linker ensures that the electrons can travel from the catecholate moiety to the Co center. Overall, MOF-1992•$[X]_n$ expands the limited number of 3D reticular frameworks that combine porosity and charge transfer, and is the first such structure to contain a functional molecular catalyst as part of the backbone.[30,31]

To study the electrochemical properties of MOF-1992•$[X]_n$, a conductive ink containing MOF-1992•$[Fe]_3$, carbon black (CB) and Nafion® was prepared and drop-casted on glassy carbon electrodes (Section S12). SEM micrographs of the MOF-1992/CB composite show high contact between MOF-1992•$[X]_n$ crystals and the carbon black (Figure S6), which serves to increase interparticle conductivity.[16] The electrochemical characterization of MOF-1992/CB cathode was performed in a three-electrode cell in a 0.1 M aqueous solution of $KHCO_3$. Cathodes prepared from MOF-1992•$[Fe]_3$ or MOF-1992•$[Mg]_3$ showed identical electrochemical features (Figure S16). This indicates that counterions inside the structures (Fe^{3+} and Mg^{2+}, respectively) are electrochemically innocent and/or substituted by K^+.

The cyclic voltammetry (CV) of MOF-1992/CB in a CO_2-saturated $KHCO_3$ solution (Figure 4a) shows a redox wave that corresponds to the sequential oxidation from CoPc-catecholate to CoPc-semiquinolate and to CoPc-quinolate (Scheme S1). The charge below the oxidation wave was used to estimate the amount of electroactive CoPc centers deposited on the cathode (Section S12). Specifically, 270 ± 35 nmol cm^{-2} of CoPc were found to be electroactive, which amounts to ~ 25 % of the total deposited CoPc. It is instructive to compare the electroactive coverage of MOF-1992/CB to that of cathodes prepared from MOF based on Zr (MOF-545Fe) or Al ($Al_2(OH)_2$TCPP-Co) (Table 1). The phthalocyanine or porphyrin active sites of the three frameworks are sterically accessible in their respective structures. However, the low conductivity associated with Al and Zr carboxylate based MOFs (< 10^{-10} S cm^{-1}) prevents high electroactive coverage. [22] The higher coverage of MOF-1992/CB (270 nmol cm^{-2}) in comparison to MOF-545Fe/CB (3 nmol cm^{-2}) confirms that carbon black only assists in the conductivity between the individual MOF crystals, as both preparations involve carbon black in the same MOF to carbon black ratio. As such, MOF-1992/CB possesses 1-2 orders of magnitude higher electroactive coverage than other cathodes based on reticular frameworks, attributable to the semiconductive and sterically accessible backbone.

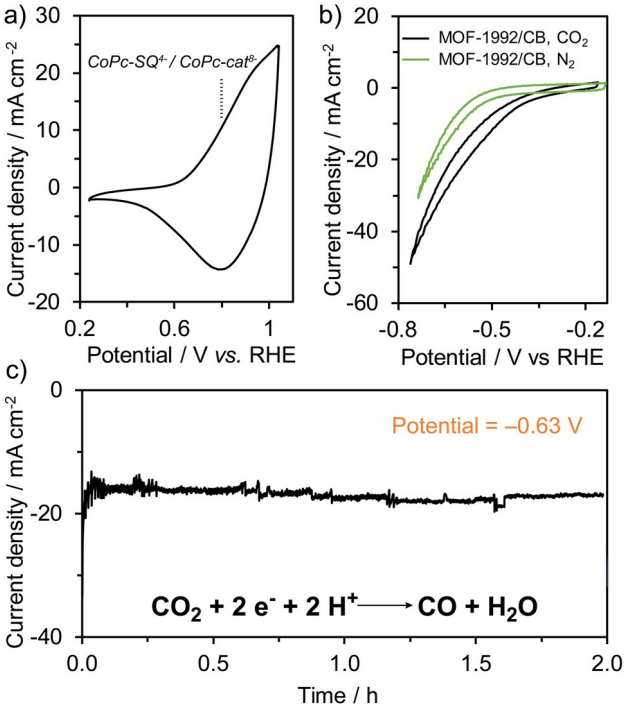

Figure 4. Electrochemical characterization of MOF-1992•$[X]_n$. a) Cyclic voltammetry (CV) for MOF-1992/CB (CB, carbon black). The vertical line shows the potential of the CoPc-semiquinolate $(CoPc\text{-}SQ)^{4-}$ / CoPc-catecholate $(CoPc\text{-}cat)^{8-}$ redox couple (b) CV for MOF-1992/CB in a CO_2-saturated (black, pH = 6.8) and N_2-saturated (green, pH = 7.2) $KHCO_3$ solution. c) Chronoamperometry at a fixed potential of −0.63 V *vs.* Reversible Hydrogen Electrode (RHE) for MOF-1992/CB in a CO_2-saturated $KHCO_3$ solution.

At cathodic potentials the CV of MOF-1992/CB shows an exponential increase of current density in a CO_2-saturated $KHCO_3$ electrolyte (Figure 4b). The CV of MOF-1992/CB displays a lower-intensity response in a N_2-saturated $KHCO_3$ electrolyte (Figure 4b). Both exponential current densities are associated with the catalytic CO_2 reduction ($CO_2 + 2\ H^+ + 2\ e^- \rightarrow CO + H_2O$) and/or H^+ reduction ($2\ H^+ + 2\ e^- \rightarrow H_2$).[8,11] To evaluate the stability of the electrocatalysis and to quantify the gaseous products, we applied a fixed potential (E = −0.63 V, overpotential = 0.52 V) to MOF-1992/CB in a CO_2-saturated solution (Figure 4c). An average current density of −16.5 ± 2.2 mA cm^{-2} was measured and the products were analyzed by gas chromatography after two hours, leading to a faradaic efficiency of 78 ± 5 % for CO and 21 ± 0.05 % for H_2 (Table S4). The fixed potential was applied for additional four hours and showed a similar faradaic efficiency (CO, 80 ± 5 %; Table S4). Over the course of the six-hour experiment, the average turnover frequency (TOF) per electroactive Co was ~ 0.20 s^{-1} (Section S12). The total turnover number (~ 5,800) compares well to that exhibited by other reticular cathodes at similar times.[16,32] A control experiment using pristine carbon black cathode under analogous conditions generated H_2 as the main product (96%; Table S6). Consequently, most of the H_2 evolution is in fact not due to the MOF-1992•$[X]_n$ catalyst but is attributed to the carbon black support.[8] SEM and CV shed light on the fate of MOF-1992/CB during electrocatalysis. SEM pictures before and after the six-hour experiment confirm the uncompromised morphology of the MOF-1992•$[X]_n$ crystals. CVs at different times (t = 0h, t = 2h, t = 6h) showed a decrease in the intensity of the catecholate redox waves but did not show the emergence of new precatalytic features (Figure S20).

Table 1. Performance in the CO_2 reduction by cathodes based on reticular frameworks

Cathode	*j* (mA cm^{-2}) *E* (V *vs.* RHE)[a]	pH	Electro. coverage (nmol cm^{-2})[b]	Main products	TOF[c] (s^{-1})	Ref.
MOF-1992/CB[d]	−16.5 (−0.63)	6.8[e]	270	CO (80 %)	0.20	this work
MOF-545Fe/CB	−1.2 (−0.60)	7.3[f]	3	CO (91 %)	0.29	16
$Al_2(OH)_2$TCPP-Co	−1.0 (−0.70)	7.3[f]	18[g]	CO (76 %)	---	15
COF-367-Co	−3.3 (−0.67)	7.3[f]	2	CO (90 %)	0.53	17

[a] Measured current density (*j*) in the applied potential (*E*),[b] Moles of electroactive catalyst/geometrical surface,[c] moles of CO/(*t* × moles of electroactive catalyst),[d] Table S4 for the associated errors,[e] 0.1 M $KHCO_3$ solution,[f] 0.5 M $KHCO_3$ solution,[g] value reestimated assuming a TOF of 0.29 s^{-1}.

The relative comparison between TOF and current density unravels the unique properties of MOF-1992 as electrocatalyst. The TOF in MOF-1992/CB is similar to the values exhibited by reticular frameworks based on porphyrin molecular catalysts at similar potentials (MOF-545Fe and COF-367-Co, Table 1). In contrast, MOF-1992 cathodes display current densities of −16.5 mA cm^{-2} at a potential of -0.63 V, which exceeds by one order of magnitude the current densities achieved by other reticular frameworks based cathodes. The high current density achieved by MOF-1992 ultimately results from the 3D semiconductive nature of the structure, which allows for a high electroactive coverage of active sites on the electrodes. Overall, MOF-1992 exemplifies how the reticulation of molecular catalysts into metal-catecholates frameworks can generate high-performing cathodes for the CO_2 reduction reaction.

ASSOCIATED CONTENT

Supporting Information

The Supporting Information is available free of charge on the ACS Publications website

General experimental methods, supplementary spectra, and analysis details (PDF)

Crystal data for MOF-1992 measured at 0.7288 Å (CIF)

Crystal data for MOF-1992 measured at 1.6085 Å (CIF)

AUTHOR INFORMATION

Present Addresses

[§]School of Advanced Materials Science and Engineering, Sungkyunkwan University (SKKU), Suwon 16419, South Korea

Corresponding Author

yaghi@berkeley.edu

Notes

The authors declare no competing financial interests.

ACKNOWLEDGMENT

We acknowledge the support from King Abdulaziz City for Science and Technology (Center of Excellence for Nanomaterials and Clean Energy Applications), Fundacion Ramon Areces (postdoctoral fellowship to R.M.), Swiss National Science Foundation (Early.Postdoc.Mobility fellowship to M.S.P) and Advanced Light Source, Lawrence Berkeley National Laboratory (beamline 12.2.1). We thank Khetpakorn Chakarawet (Mössbauer spectroscopy) and Jeffrey Derrick (gas chromatography) for assistance in data collection. We thank QB3 Biomolecular Nanotechnology Center and staff for assistance in XPS data collection. J.K acknowledges IBS Global Postdoctoral Fellowship (IBS-R026-D1).

REFERENCES

(1) Armstrong, R. C.; Wolfram, C.; de Jong, K. P.; Gross, R.; Lewis, N. S.; Boardman, B.; Ragauskas, A. J.; Ehrhardt-Martinez, K.; Crabtree, G.; Ramana, M. V. The Frontiers of Energy. *Nat. Energy* **2016**, *1*, 15020.
(2) Montoya, J. H.; Seitz, L. C.; Chakthranont, P.; Vojvodic, A.; Jaramillo, T. F.; Nørskov, J. K. Materials for Solar Fuels and Chemicals. *Nat. Mater.* **2016**, *16*, 70.
(3) De Luna, P.; Hahn, C.; Higgins, D.; Jaffer, S. A.; Jaramillo, T. F.; Sargent, E. H. What Would It Take for Renewably Powered Electrosynthesis to Displace Petrochemical Processes? *Science* **2019**, *364* (6438), eaav3506.
(4) Weng, Z.; Jiang, J.; Wu, Y.; Wu, Z.; Guo, X.; Materna, K. L.; Liu, W.; Batista, V. S.; Brudvig, G. W.; Wang, H. Electrochemical CO_2 Reduction to Hydrocarbons on a Heterogeneous Molecular Cu Catalyst in Aqueous Solution. *J. Am. Chem. Soc.* **2016**, *138* (26), 8076–8079.
(5) Costentin, C.; Drouet, S.; Robert, M.; Savéant, J.-M. A Local Proton Source Enhances CO_2 Electroreduction to CO by a Molecular Fe Catalyst. *Science* **2012**, *338* (6103), 90 LP-94.
(6) Beley, M.; Collin, J. P.; Ruppert, R.; Sauvage, J. P. Electrocatalytic Reduction of Carbon Dioxide by Nickel Cyclam^{2+} in Water: Study of the Factors Affecting the Efficiency and the Selectivity of the Process. *J. Am. Chem. Soc.* **1986**, *108* (24), 7461–7467.
(7) Froehlich, J. D.; Kubiak, C. P. The Homogeneous Reduction of CO_2 by [Ni(Cyclam)]$^+$: Increased Catalytic Rates with the Addition of a CO Scavenger. *J. Am. Chem. Soc.* **2015**, *137* (10), 3565–3573.
(8) Zhang, X.; Wu, Z.; Zhang, X.; Li, L.; Li, Y.; Xu, H.; Li, X.; Yu, X.; Zhang, Z.; Liang, Y.; Wang, H. Highly Selective and Active CO_2 Reduction Electrocatalysts Based on Cobalt Phthalocyanine/Carbon Nanotube Hybrid Structures. *Nat. Commun.* **2017**, *8*, 14675.
(9) Wang, M.; Torbensen, K.; Salvatore, D.; Ren, S.; Joulié, D.; Dumoulin, F.; Mendoza, D.; Lassalle-Kaiser, B.; Işci, U.; Berlinguette, C. P.; Robert, M. CO_2 Electrochemical Catalytic Reduction with a Highly Active Cobalt Phthalocyanine. *Nat. Commun.* **2019**, *10* (1), 3602.
(10) Tatin, A.; Comminges, C.; Kokoh, B.; Costentin, C.; Robert, M.; Savéant, J.-M. Efficient Electrolyzer for CO_2 Splitting in Neutral Water Using Earth-Abundant Materials. *Proc. Natl. Acad. Sci.* **2016**, *113* (20), 5526 LP-5529.
(11) Ren, S.; Joulié, D.; Salvatore, D.; Torbensen, K.; Wang, M.; Robert, M.; Berlinguette, C. P. Molecular Electrocatalysts Can Mediate Fast, Selective CO_2 Reduction in a Flow Cell. *Science* **2019**, *365* (6451), 367 LP-369.
(12) Yaghi, O.; Kalmutzki, M.; Diercks, C. *Introduction to Reticular Chemistry: Metal-Organic Frameworks and Covalent Organic Frameworks*; Wiley-VCH Verlag GmbH & Co. KGaA: Weinheim, Germany, 2019.
(13) Diercks, C. S.; Liu, Y.; Cordova, K. E.; Yaghi, O. M. The Role of Reticular Chemistry in the Design of CO_2 Reduction Catalysts. *Nat. Mater.* **2018**, *17* (4), 301–307.
(14) Hod, I.; Sampson, M. D.; Deria, P.; Kubiak, C. P.; Farha, O. K.; Hupp, J. T. Fe-Porphyrin-Based Metal–Organic Framework Films as High-Surface Concentration, Heterogeneous Catalysts for Electrochemical Reduction of CO_2. *ACS Catal.* **2015**, *5* (11), 6302–6309.
(15) Kornienko, N.; Zhao, Y.; Kley, C. S.; Zhu, C.; Kim, D.; Lin, S.; Chang, C. J.; Yaghi, O. M.; Yang, P. Metal–Organic Frameworks for Electrocatalytic Reduction of Carbon Dioxide. *J. Am. Chem. Soc.* **2015**, *137* (44), 14129–14135.
(16) Dong, B.-X.; Qian, S.-L.; Bu, F.-Y.; Wu, Y.-C.; Feng, L.-G.; Teng, Y.-L.; Liu, W.-L.; Li, Z.-W. Electrochemical Reduction of CO_2 to CO by a Heterogeneous Catalyst of Fe–Porphyrin-Based Metal–Organic Framework. *ACS Appl. Energy Mater.* **2018**, *1* (9), 4662–4669.
(17) Lin, S.; Diercks, C. S.; Zhang, Y. B.; Kornienko, N.; Nichols, E. M.; Zhao, Y.; Paris, A. R.; Kim, D.; Yang, P.; Yaghi, O. M. Chang, C. Covalent Organic Frameworks Comprising Cobalt Porphyrins for Catalytic CO_2 Reduction in Water. *Science* **2015**, *349* (6253), 1208–1213.
(18) Cheung, P. L.; Lee, S. K.; Kubiak, C. P. Facile Solvent-Free Synthesis of Thin Iron Porphyrin COFs on Carbon Cloth Electrodes for CO_2 Reduction. *Chem. Mater.* **2019**, *31* (6), 1908–1919.
(19) Nguyen, N. T. T.; Furukawa, H.; Gándara, F.; Trickett, C. A.; Jeong, H. M.; Cordova, K. E.; Yaghi, O. M. Three-Dimensional Metal-Catecholate Frameworks and Their Ultrahigh Proton Conductivity. *J. Am. Chem. Soc.* **2015**, *137*, 15394–15397.
(20) Hmadeh, M.; Lu, Z.; Liu, Z.; Gándara, F.; Furukawa, H.; Wan, S.; Augustyn, V.; Chang, R.; Liao, L.; Zhou, F.; Perre, E.; Ozolins, V.; Suenaga, K.; Duan, X.; Dunn, B.; Yamamto, Y.; Terasaki, O.; Yaghi, O. New Porous Crystals of Extended Metal-Catecholates. *Chem. Mater.* **2012**, *24* (18), 3511–3513.
(21) DeGayner, J. A.; Jeon, I.-R.; Sun, L.; Dincă, M.; Harris, T. D. 2D Conductive Iron-Quinoid Magnets Ordering up to Tc = 105 K via Heterogenous Redox Chemistry. *J. Am. Chem. Soc.* **2017**, *139* (11), 4175–4184.
(22) Sun, L.; Campbell, M. G.; Dincă, M. Electrically Conductive Porous Metal–Organic Frameworks. *Angew. Chemie Int. Ed.* **2016**, *55* (11), 3566–3579.
(23) Meshitsuka, S.; Ichikawa, M.; Tamaru, K. Electrocatalysis by Metal Phthalocyanines in the Reduction of Carbon Dioxide. *J. Chem. Soc.{,} Chem. Commun.* **1974**, No. 5, 158–159.
(24) Kramer, W. W.; McCrory, C. C. L. Polymer Coordination Promotes Selective CO_2 Reduction by Cobalt Phthalocyanine. *Chem. Sci.* **2016**, *7* (4), 2506–2515.
(25) Zhong, H.; Ly, K. H.; Wang, M.; Krupskaya, Y.; Han, X.; Zhang, J.; Zhang, J.; Kataev, V.; Büchner, B.; Weidinger, I. M.; Kaskel, S.; Liu, P.; Chen, M.; Dong, R.; Feng, X. A Phthalocyanine-Based Layered Two-Dimensional Conjugated Metal–Organic Framework as a Highly Efficient Electrocatalyst for the Oxygen Reduction Reaction. *Angew. Chemie - Int. Ed.* **2019**, *58* (31), 10677–10682.
(26) Spitler, E. L.; Dichtel, W. R. Lewis Acid-Catalysed Formation of Two-Dimensional Phthalocyanine Covalent Organic Frameworks. *Nat. Chem.* **2010**, *2*, 672.
(27) Nagatomi, H.; Yanai, N.; Yamada, T.; Shiraishi, K.; Kimizuka, N. Synthesis and Electric Properties of a Two-Dimensional Metal-Organic Framework Based on Phthalocyanine. *Chem. – A Eur. J.* **2018**, *24* (8), 1806–1810.
(28) Meng, Z.; Aykanat, A.; Mirica, K. A. Welding Metallophthalocyanines into Bimetallic Molecular Meshes for Ultrasensitive, Low-Power Chemiresistive Detection of Gases. *J. Am. Chem. Soc.* **2019**, *141* (5), 2046–2053.
(29) Lei, T.; Lai, M.; Kong, Q.; Lu, D.; Lee, W.; Dou, L.; Wu, V.; Yu, Y.; Yang, P. Electrical and Optical Tunability in All-Inorganic Halide Perovskite Alloy Nanowires. *Nano Lett.* **2018**, *18* (6), 3538–3542.
(30) Xie, L. S.; Sun, L.; Wan, R.; Park, S. S.; DeGayner, J. A.; Hendon, C. H.; Dincă, M. Tunable Mixed-Valence Doping toward Record Electrical Conductivity in a Three-Dimensional Metal–Organic Framework. *J. Am. Chem. Soc.* **2018**, *140* (24), 7411–7414.
(31) Aubrey, M. L.; Wiers, B. M.; Andrews, S. C.; Sakurai, T.; Reyes-Lillo, S. E.; Hamed, S. M.; Yu, C.-J.; Darago, L. E.; Mason, J. A.; Baeg, J.-O.; Grandjean, F.; Long, G. J.; Seki, S.; Neaton, J. B.; Yang, P.; Long, J. R. Electron Delocalization and Charge Mobility as a Function of Reduction in a Metal–organic Framework. *Nat. Mater.* **2018**, *17* (7), 625–632.
(32) Diercks, C. S.; Lin, S.; Kornienko, N.; Kapustin, E. A.; Nichols, E. M.; Zhu, C.; Zhao, Y.; Chang, C. J.; Yaghi, O. M. Reticular Electronic Tuning of Porphyrin Active Sites in Covalent Organic Frameworks for Electrocatalytic Carbon Dioxide Reduction. *J. Am. Chem. Soc.* **2018**, *140* (3), 1116–1122.

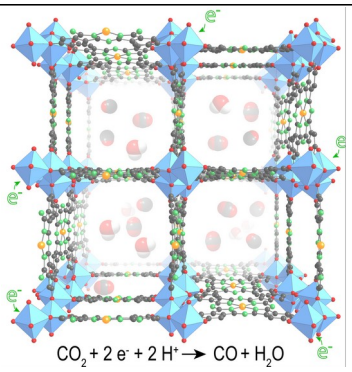

metal-catecholate framework, metal-organic framework, conductive MOFs, CO_2 reduction, electrocatalysis